Reaction of methylidyne CH(X²Π) radical with CH_4 and H_2S: overall rate constant and absolute atomic hydrogen production

Paul Fleurat-Lessard, Jean-Claude Rayez, Astrid Bergeat,
Jean-Christophe Loison*

Laboratoire de Physico-Chimie Moléculaire, CNRS UMR 5803, Université Bordeaux I, F-33405 Talence Cedex, France

Abstract

The $CH + CH_4$ and H_2S reactions were studied, at room temperature, in a low-pressure fast-flow reactor. $CH(X^2\Pi, v = 0)$ radicals were obtained from the reaction of $CHBr_3$ with potassium atoms. The overall rate constants were found at 330 K to be $(0.76 \pm 0.20) \times 10^{-10}$ and $(2.8 \pm 0.8) \times 10^{-10}$ cm^3 $molecule^{-1}$ s^{-1}, respectively. The absolute atomic hydrogen productions were determined by resonance fluorescence in the vacuum ultraviolet: H production from the $CH + CH_4$ reaction is 100% and from the $CH + H_2S$ reaction is $99^{+1}_{-4}\%$, the H production from the $CH + H_2$ reaction being the reference. Ab initio studies of the different stationary points relevant to the $CH + CH_4$ reaction have been performed at the CCSD(T)/cc-pVTZ level and comparison is made with experimental results. The experimental results for the $CH + H_2S$ reaction is compared with those of a recent theoretical study [Chem. Phys. 242 (1999) 1]. © 2002 Elsevier Science B.V. All rights reserved.
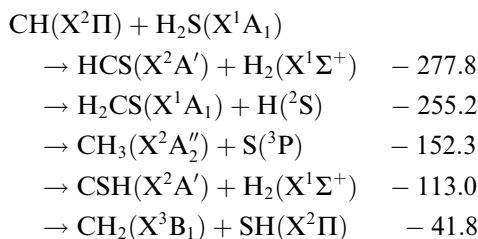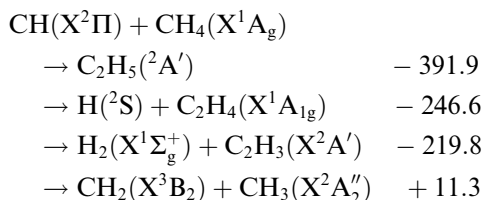
1. Introduction

The CH radical is one of the most reactive radical, and it is well known as an important intermediate in various reaction systems in fields from planetary atmospheres to hydrocarbon combustion [1]. This unusually high reactivity is due to the presence of one singly occupied and one vacant non-bonding molecular orbital localized on the C atom, allowing addition on π-bonds and insertion in σ-bonds with no barrier. For example, the $CH + CH_4$ reaction is important for the Titan atmosphere chemistry [2], and CH reactions are very important for the NO_x production during combustion process [3]. The $CH + H_2S$ reaction is a typical H_2X-type reaction and is thus a prototype of the $CH + H_2O$ reaction. This reaction is also an important reaction for combustion of oil and coals, and may also be concerning by sulfur interstellar chemistry. Despite their importance, there was, to our knowledge, no experimental study of the product branching ratio for these two reactions of CH with CH_4 or H_2S.

---

* Corresponding author. Fax: +33-5-57-96-2521.
E-mail address: jc@lpcm.u-bordeaux.fr (J.-C. Loison).

The possible reaction channels are ($\Delta_r H^0$ in kJ mol^{-1}) [4–10]:

$$CH(X^2\Pi) + CH_4(X^1A_g)$$

$\rightarrow C_2H_5(^2A')$	-391.9
$\rightarrow H(^2S) + C_2H_4(X^1A_{1g})$	-246.6
$\rightarrow H_2(X^1\Sigma_g^+) + C_2H_3(X^2A')$	-219.8
$\rightarrow CH_2(X^3B_2) + CH_3(X^2A_2'')$	$+11.3$

$$CH(X^2\Pi) + H_2S(X^1A_1)$$

$\rightarrow HCS(X^2A') + H_2(X^1\Sigma^+)$	-277.8
$\rightarrow H_2CS(X^1A_1) + H(^2S)$	-255.2
$\rightarrow CH_3(X^2A_2'') + S(^3P)$	-152.3
$\rightarrow CSH(X^2A') + H_2(X^1\Sigma^+)$	-113.0
$\rightarrow CH_2(X^3B_1) + SH(X^2\Pi)$	-41.8

Many experiments have been carried out to determine the overall rate constant of the $CH + CH_4$ reaction with various techniques [11]. At 300 K, there is a general agreement with a rate constant of about 9×10^{-11} cm^3 molecule^{-1} s^{-1}, and a significant temperature dependence over the range 13–770 K [12,13]. In contrast with the fact that the overall rate constant has been accurately determined over a wide range of temperature, few is available about the product branching ratios, although they are needed to model the combustion or interstellar chemistry processes. It has been commonly accepted that the $CH + CH_4$ reaction could only lead to $H + C_2H_4$ products at low pressure, the stabilization of the C_2H_5 ethyl radical being estimated negligible below 10^5 Torr [13], and the slightly endothermic channel $CH_2 + CH_3$ being negligible below 2000 K [13]. However no experimental studies have been performed to confirm it, and the various ab initio calculations do not totally rule out the possibility of the $C_2H_3 + H_2$ channel.

Sato et al. [10] have recently determined the overall rate constant of the $CH + H_2S$ reaction at room temperature associated with ab initio and RRKM studies on the branching ratios. The rate constant was found to be $(3.2 \pm 0.8) \times 10^{-10}$ cm^3 molecule^{-1} s^{-1} and the RRKM calculations suggest that the main product channel is $H_2CS + H$.

In order to have a better understanding of the mechanism of the title reactions, we have performed new kinetics experiments using a selective source of CH radicals (from the reaction of $CHBr_3$ with potassium atoms), in a low-pressure fast-flow reactor at room temperature. The overall rate constants were determined by following the decay of the CH radicals laser induced fluorescence signal, the methane or the hydrogen sulfide being introduced in excess, the diffusion corrections having been validated in a previous study. Absolute product branching ratios were estimated over the channels yielding H atoms by comparison with the $CH + H_2 \rightarrow CH_2 + H$ reaction [14,15], H atoms being probed by resonance fluorescence in the vacuum ultraviolet. New ab initio studies were thus performed in order to assess more precisely the role of the $CH + CH_4 \rightarrow C_2H_3 + H_2$ reaction channel. The use of the $CH + CH_4$ reaction for calibration of hydrogen atoms production yield in CH reactions is discussed.

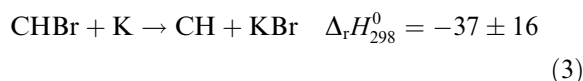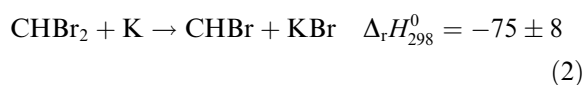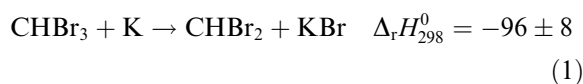## 2. Theoritical and experimental methodology

2.1. Ab initio calculations

Stationary points along the $CH(X^2\Pi) + CH_4$ (X^1A_g) reaction path have first been found using the coupled cluster method including single and double excitations and a perturbational estimate of triple excitations, CCSD(T) [15], with the correlation consistent polarized valence double zeta (cc-pVDZ) basis set of Dunning [17]. The harmonic vibrational wavenumbers have been computed at the same level of theory in order to characterize the stationary points as minima or saddle points and to obtain zero-point vibrational energy (ZPVE). Structures and total energies were then refined at the CCSD(T)/cc-pVTZ level [16,17], using the restricted open shell formalism. ZPVE correction to energies is used without any scaling factor. Unless otherwise noted, the discussed energetics are those obtained at the CCSD(T)/cc-pVTZ with CCSD(T)/cc-pVDZ ZPVE corrections. For CCSD(T) calculations the core electrons have been frozen. All CCSD(T)/cc-pVDZ calculations have been carried out with the Gaussian 98 program [18], and all CCSD(T)/cc-pVTZ calculations have been carried out with the Molpro 2000.1 program [19–21].

2.2. Experimental measurements

The experimental setup has been described in detail previously [22–24], and only a summary is given here. The setup consists of a fast-flow reactor, i.e., a 36-mm inner tube with four optical ports for detection. The CH radicals are produced in an "injector" which slides in the reactor. At the end of the injector, the CH radicals are mixed with the methane or hydrogen sulfide flow. Then, the distance between the end of the injector and the observation windows is directly proportional to the reaction time. The distance (d) between the windows detection and the injector nozzle aperture could be varied over the range 0–100 mm with 0.5-mm precision. The pressure was measured by a capacitance manometer (Barocel 0–10 Torr) and the flow rates were adjusted by thermal mass flow meters. Before each experiment, the vacuum and the leak-plus-out gassing rate were checked with a Pirani gauge (respectively, <0.05 and <10 mTorr min^{-1}).

The CH radicals were produced in the reactant injector nozzle from the CHBr$_3$ + 3K → CH + 3KBr overall reaction which can be separated into the elementary steps ($\Delta_r H^0$ in kJ mol^{-1} [25]):

$$CHBr_3 + K \rightarrow CHBr_2 + KBr \quad \Delta_r H^0_{298} = -96 \pm 8 \tag{1}$$

$$CHBr_2 + K \rightarrow CHBr + KBr \quad \Delta_r H^0_{298} = -75 \pm 8 \tag{2}$$

$$CHBr + K \rightarrow CH + KBr \quad \Delta_r H^0_{298} = -37 \pm 16 \tag{3}$$

As all the K + CHBr$_x$ → KH + CBr$_x$ ($x \geqslant 0$) reactions are endoergic, this source can only produce CH radicals. As the sum of the exothermicities of the three abstractions is 208 kJ mol^{-1}, the production of CH($a^4\Sigma^-$) radicals, which is 69.9 kJ mol^{-1} above the ground state, is possible. However, as the last Br abstraction is only 37 kJ mol^{-1} above the ground state, production of CH($a^4\Sigma^-$) requires high concentration of meta-stable electronic excited CHBr in the oven, which is unlikely. Moreover, the CH($a^4\Sigma^-$) reactivity is

much lower than the CH($X^2\Pi$) reactivity toward CH$_4$, H$_2$ and H$_2$O (and then H$_2$S) [26] and thus will not contribute to H production. Additionally LIF detection of CH($X^2\Pi$) radical, using a ND:YAG laser (Quantel YG 581C) pumped dye laser and exciting the CH($A^2\Delta \leftarrow X^2\Pi$) near 431 nm, allow us to determine that the CH($X^2\Pi$) is fully vibrationally and rotationally relaxed.

The CHBr$_3$, diluted in He, is mixed inside the injector with potassium vapor, coming from a micro furnace [22]. The injector conditions are the following: $P = 1.4$ Torr, [K] = 1 mTorr, [CHBr$_3$] = 0.05 mTorr, which give in the fast-flow reactor: $P = 1.4$ Torr, [K] < 0.1 mTorr, [CHBr$_3$, CHBr$_2$, CHBr] $\ll 0.001$ mTorr and [CH] ≈ 0.003 mTorr. As a large excess of potassium is introduced in the injector compared to the CHBr$_3$ concentration, the precursors (CHBr$_3$, CHBr$_2$, CHBr) concentrations in the fast-flow reactor are very small. The difference between CH concentration in the fast-flow reactor and CHBr$_3$ concentration introduced is due to wall reactions in the micro furnace leading to 30% efficiency conversion, and dilution of the injector flow in the reactor. As the K + H$_2$S reaction presents a barrier in the gas phase, the only possible reaction of K atoms leads to the formation of an adduct, which is absolutely negligible in our low-pressure experimental conditions.

CH$_4$ and H$_2$S were used directly from the cylinders with a purity >99.995% for CH$_4$ and >97.5% for H$_2$S (the main impurities were CS$_2$ and OCS below 2000 ppv). CHBr$_3$ (99%) was used without any further purification.

Hydrogen atoms were detected by their resonance fluorescence using the $2p^1 \, ^2P^0 \leftrightarrow 1s^1 \, ^2S$ transition at 121.6 nm. Atom excitation was achieved with the microwave discharge lamp previously used to probe the atomic products of the CH + NO reaction [27]. A pure helium flow (purity of 99.9999%) was used for the branching ratio determination. The general procedure for atomic detection has also been detailed previously [23,27]. We would only mention that the conditions of the presently reported experiments ensure the linear dependence of the atomic fluorescence versus both the lamp emission intensity and the H atoms concentration.

3. Results

3.1. Potential energy surface

The CCSD(T)/cc-pVTZ optimized structures of the different minima and transition structures lying on the doublet surface are displayed in Fig. 1 together with the available experimental values [4–9,30,36], while the energy diagram along the reaction path is shown in Fig. 2.

3.1.1. Geometries
3.1.1.1. Reactants and products. Experimentally determined geometries are available for each reactant and product. For the ethyl radical, only the C–C bond distance is known from recent laser
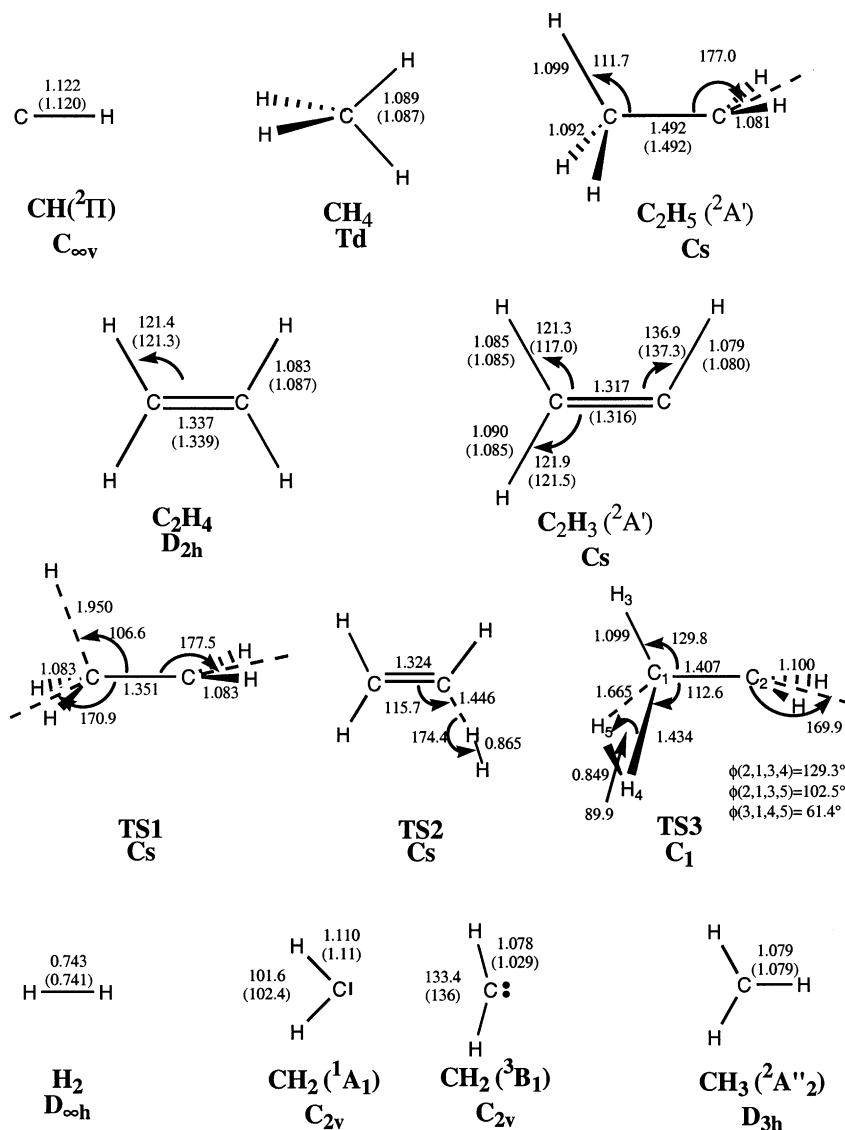

Fig. 1. Optimized geometries. Distances in Å and angles in degrees. Experimental values are indicated in parenthesis. For TS3, the parameters are those obtained at the CCSD(T)/cc-pVDZ level.
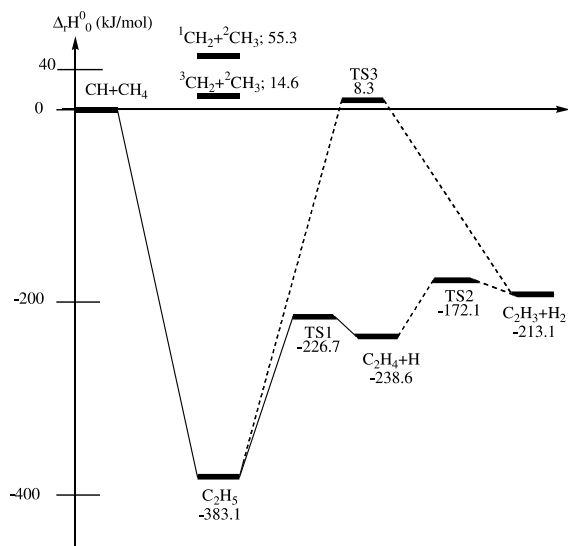
Fig. 2. Schematic picture of the potential energy surface (PES) correlating with methylidyne $CH(X^2\Pi)$ and methane CH_4 (X^1A_g) ground states.

spectroscopy experiments [30]. For all the geometric parameters, agreement between the CCSD(T)/cc-pVTZ optimized geometries (Fig. 1) and experimental values are within 0.02 Å for bond lengths and 1.0° for bond angles.

Moreover, the agreement with earlier theoretical results at similar levels of calculation is very good: on the average, the bond distances differ by less than 0.005 Å and the bond angles by less than 0.1° [28,29,31–35,37].

3.1.1.2. Transition states. The transition state TS1 is depicted in Fig. 1 and Table 1. It corresponds to an hydrogen loss from the ethyl radical. It has C_s symmetry with the mirror plane containing the two carbon atoms and the departing hydrogen atom. The structure of this transition state corresponds to a late barrier: the geometry of the C_2H_4 fragment nearly coincides with that of the free ethylene molecule, and the leaving H atom is about 2 Å away. This late character is in accord with the

Table 1
Main structural parameters for TS1

	UMP2 6-31G(d,p)[a]	QCISD 6-311G(d,p)[b]	QCISD(T) 6-311G(d,p)[c]	CCSD(T) VTZ[d]
d(CC)	1.335	1.353	1.357	1.351
$d(CH_a)$	1.865	1.976	1.967	1.950
$d(CH_b)$	1.079	1.087	1.088	1.083
$d(CH_c)$	1.079	1.087	1.088	1.083
$\alpha(CCH_a)$	107.2	106.7	106.7	106.6
$\alpha(CCH_b)$	121.5	121.1	–[e]	121.1
$\alpha(CCH_c)$	121.5	121.4	–	121.3
$\Theta(H_aCCH_b)$	±96.7	±95.9	–	±95.5
$\Theta(H_aCCH_c)$	±88.3	±88.7	–	±88.5
Barrier height (relative to C_2H_5)	180.9[f]	167.9[g]	155.7[h]	156.2[i]

Distances in Å and angles in degrees. Barrier height in kJ mol^{-1}.
[a] From [33].
[b] From [28,31,32].
[c] From [34].
[d] This work. Absolute electronic energy: −78.934182 a.u.
[e] A – indicates that this value is not given in the original article.
[f] ZPVE: UMP2/6-31G(d,p).
[g] ZPVE: QCISD/6-311G(d,p).
[h] ZPVE: MP2/6-31G(d,p).
[i] ZPVE: CCSD(T)/cc-pVDZ.

reaction endothermicity (144 kJ mol^{-1} at our level of calculations, see below). Agreement with previous theoretical studies is good [8,28,32,33].
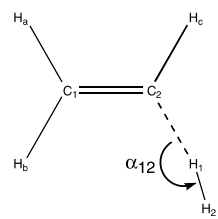
TS2 is the transition state for the abstraction reaction $C_2H_4 + H \rightarrow C_2H_3 + H_2$. It possesses a planar geometry and its main structural parameters are shown in Table 2. This structure can be described as a H_2 molecule departing from a C_2H_3 radical; at our level of calculation, the distance between the carbon atom and the first hydrogen atom in this transition state is 1.45 Å, longer by 0.35 Å than a typical C–H bond length. Meanwhile, the H–H bond in H_2 is elongated only by 0.13 Å, as compared with the free H_2 (0.741 Å) [38]. This transition state has a late character; in agreement with the endothermicity of this reaction (26 kJ mol^{-1}, see below). Agreement with previous theoretical studies is good [8,28].

TS3 is the transition state for 1,1-elimination of a H_2 molecule from the ethyl radical: $C_2H_5 \rightarrow C_2H_3 + H_2$.

It is worth noting that Morokuma and co-workers [28] have unsuccessfully searched this transition state within the C_s symmetry. The transition state structures they obtained correspond to an excited electronic state and further optimization of these structures without any symmetry constraint leads to either TS1 or TS2. This is in agreement with the fact that, as predicted by a Woodward–Hoffman correlation diagram, the ground state of the ethyl radical could not lead to the ground state of $C_2H_3 + H_2$ under the C_s symmetry constraint (see Appendix A).

Therefore, we have undergone the search for a direct H_2-elimination without any symmetry constraint. However, as the TS1 and TS2 structures

Table 2
Main structural parameters for TS2

	MP2 6-31G(d,p)[a]	QCISD 6-311G(d,p)[b]	CCSD(T) VTZ[c]
d(CC)	1.290	1.326	1.324
d(CH$_1$)	1.444	1.427	1.446
d(H$_1$H$_2$)	0.848	0.872	0.865
α_{12}	175.6	175.9	174.4
d(CH$_a$)	1.084	1.091	1.087
d(CH$_b$)	1.082	1.088	1.084
d(CH$_c$)	1.080	1.086	1.082
α(CCH$_a$)	121.8	_[d]	121.3
α(CCH$_b$)	121.5	–	121.6
α(CCH$_c$)	131.5	130.8	131.0
α(CCH$_1$)	115.7	115.6	115.7
Barrier height (relative to $C_2H_4 + H$)	65.2[e]	73.7[f]	66.6[g]

Distances in Å and angles in degrees. Barrier height in kJ mol^{-1}. (e) From [34].
[a] From [8].
[b] From [28].
[c] This work. Absolute electronic energy: −78.91084 a.u.
[d] A – indicates that this value is not given in the original article.
[e] ZPVE: MP2/6-31G(d,p).
[f] ZPVE: MP2/6-31G(d,p) scaled by 0.95.
[g] ZPVE: CCSD(T)/cc-pVDZ.

are much lower in energy than the expected transition state, a direct unconstraint geometry optimization starting from an approximate structure will eventually lead to either TS1 or TS2. We have thus started from a structure derived from that of the 1,1-H_2 elimination from ethane [42]. In order to prevent the optimization to lead to the more stable structures TS1 or TS2, we have first frozen the departing H_2 molecule, while optimizing only the C_2H_3 fragment. Starting from the resulting structure, we have then done a full optimization which led to TS3. However, as this structure is located much higher in energy than TS1 or TS2, its geometry was optimized at the CCSD(T)/cc-pVDZ level only. We have then performed a single point calculation using this geometry at the CCSD(T)/cc-pVTZ level. The main structural parameters are shown in Fig. 1.

This transition state is better described as a H_2 molecule departing from the C_2H_5 radical. As in the ethyl radical, the remaining C_2H_3 fragment is non-planar, which corresponds to a distorted structure compared to the equilibrium geometry of the vinyl radical. This transition state corresponds to an asymmetric process, one C–H bond (C_1H_5) being much longer than the other one (C_1H_4): 1.665 Å compared to 1.434 Å. As in the TS2 structure, these distances are much longer than a typical C–H bond. The H–H bond in H_2 is equal to 0.849 Å, which is similar to that found in the transition state TS2: 0.865 Å.

3.1.2. Relative stability and thermochemistry

The energy diagram along the reaction path is shown in Fig. 2. The experimental enthalpies of formation at 0 K, $\Delta_f H_0^0$, from [4–9] are reported in Table 3. Using these enthalpies, the relative stability of the main species can be estimated. In Table 4, the experimental heats of reaction at 0 K ($\Delta_r H_0^0$) are compared to those obtained at the CCSD(T)/cc-pVTZ level. At this level, computed values for each $\Delta_r H_0^0$ are within 9 kJ mol^{-1} of the literature values, the RMS error being 5 kJ mol^{-1}. It is worth noting that the error on relative energies of $C_2H_4 + H$ and $C_2H_3 + H_2$ towards C_2H_5 is less than 2 kJ mol^{-1}. The larger error on the relative energy of C_2H_5 towards CH + CH$_4$ could come from the multireference character of the

Table 3
Experimental enthalpies of formation at 0 K, in kJ mol^{-1}

	Experimental $\Delta_f H^0$ at 0 K (kJ mol^{-1})
CH($^2\Pi$)	590.8[a]
CH$_4$	−67.0[a]
C$_2$H$_5$(^{2}A′)	131.9 ± 2.1[b,c]
C$_2$H$_4$	61.1[a]
C$_2$H$_3$(^{2}A′)	304.0 ± 3.3[b,d]
CH$_2$(^{3}B$_1$)	386.0[a]
CH$_3$(^{2}A″$_2$)	149.0[a]
H	216.0[a]

[a] From [4].
[b] From [5].
[c] From [9].
[d] From [6–8].

Table 4
Experimental and calculated enthalpies of formation at 0 K, in kJ mol^{-1}

Species	Experimental (0 K)	This work (0 K)
CH($^2\Pi$) + CH$_4$	0	0[a]
C$_2$H$_5$(^{2}A′)	−391.9 ± 2.1[b]	−383.1
TS1	−232.8[c]	−226.7
C$_2$H$_4$ + H	−246.6[b]	−238.6
TS2	−176.3[d]	−172.1
C$_2$H$_3$ + H$_2$	−219.8 ± 3.3[b]	−213.1
TS3		+8.3
CH$_2$(^{3}B$_1$)+ CH$_3$(^{2}A″$_2$)	11.3[b]	14.6

[a] Absolute electronic energy: −78.84834 a.u.
[b] From Table 6.
[c] From [41].
[d] From [28].

CH($^2\Pi$) molecule. However, the value of the T1(CCSD) diagnostic, which gives an indication of the validity of the correlation method based on a single reference [39,40], has been computed to be always less than recommended value of 0.02 [40], even in the case of the open shell molecules.

3.1.3. Reaction mechanism

Fig. 2 displays a schematic picture of the potential energy surface (PES) correlating with methylidyne CH(X$^2\Pi$) and methane CH$_4$(X^{1}A$_1$) ground states. On the entrance channel, the ethyl radical C$_2$H$_5$ is formed without any barrier. This is in agreement with the large rate constant at low

temperature and shows the ability of CH radical to insert into a C–H bond. Starting from the ethyl radical, several channels are conceivable. First, the C–C bond can dissociate to form the $CH_2(^3B_1)$ and $CH_3(^2A_2'')$ fragments. However, as seen in the previous part, this channel is endothermic. Second, loss of an hydrogen atom could lead to $CH_2CH_2 +$ H or $CH_3CH +$ H. Between these two channels, only the first one is exothermic, the second one being endothermic by at least 500 kJ mol^{-1} at the CCSD(T)/cc-pVDZ level; the singlet ($^1A'$) and triplet ($^3A''$) CH_3CH isomers lie, respectively, 750 and 880 kJ mol^{-1} higher in energy than the ethylene form. As the reaction leading to $CH_3CH +$ H is largely endothermic (at least 540 kJ mol^{-1}), it is not considered further. A transition state (TS1) is located connecting the ethyl radical to an ethylene molecule and a hydrogen atom. The energy barrier is 156.2 kJ mol^{-1}; the relative energy of TS1 being -226.7 kJ mol^{-1} with respect to the entrance channel. This channel is much lower in energy than the dissociation of the C–C bond, and should have a larger contribution. The value of the energy barrier is in very good agreement with the experimental values deduced from a Transition State modeling of the dissociation. Berman and Lin [41] estimated a barrier height of 159 kJ mol^{-1}, while Hase et al. [31] found a barrier of 158 kJ mol^{-1}. In a second step, the hydrogen atom can abstract a second hydrogen atom from C_2H_4 to form the vinyl radical C_2H_3 and a hydrogen molecule H_2. The barrier height for this abstraction reaction is equal to 67 kJ mol^{-1} at the CCSD(T)/cc-pVTZ level at 0 K. This value is in good agreement with the experimental value of 65 kJ mol^{-1}. This experimental value corresponds to the value of 63 kJ mol^{-1} obtained by Knyasev et al. [8] at 298 K and extrapolated to 0 K using the thermal energy calculated at the CCSD(T)/cc-pVDZ level. (Conversely, the barrier height at 298 K equals 64 kJ mol^{-1} at the CCSD(T)/cc-pVTZ level, in good agreement with the original value of Knyasev et al.) Our energy barrier is about 8 kJ mol^{-1} lower than the previous calculations of Morokuma and co-workers [28]: 74 kJ mol^{-1} at the CCSD(T)/cc-pVTZ// QCISD(T)/6-311G(d,p) and QCISD(T)/6-311G (d,p) levels, using the MP2/6-31G(d,p) ZPVE scaled by 0.95. This overestimation has already

been pointed out by Knyasev et al. [8] who underlined that a better agreement with their experimental data was found by lowering these values by 5 to 68.6 kJ mol^{-1}. It is worth noting that, as the $C_2H_4 +$ H channel is open, the hydrogen atom will go away and, although the transition state TS2 is located 172.0 kJ mol^{-1} below the entrance channel, this second step will be inaccessible.

Starting from the ethyl radical, the other channel is the loss of a H_2 molecule leading to $C_2H_3 + H_2$. Two distinct paths would also be possible; 1,1-H_2 loss where the two departing hydrogen atoms are from the same carbon atom and 1,2-H_2 loss where the hydrogen atoms come from different carbon atoms. The 1,1-H_2 loss can lead to $HCCH_2 + H_2$ or $H_3CC + H_2$ isomers. The $CH_3C(^2A')$ and $CH_3C(^4A'')$ species are located 200 and 328 kJ mol^{-1} higher in energy than the CH_2CH ground state, which means that their relative energies towards $CH + CH_4$ are, respectively, -12 kJ mol^{-1} ($^2A'$) and 114 kJ mol^{-1} ($^4A''$). Although the reaction leading to the $CH_3C(^2A')$ isomer is exothermic, the loss of a H_2 molecule corresponds to an important electronic reorganization and should proceed through a transition state high in energy. Therefore, none of these isomers is considered further.

As the H_2 molecule leaves the C_2H_3 moiety, there is a formation of a π_{C-C} bond, as in the elimination of H_2 from ethane to form $C_2H_4 + H_2$. Therefore, the activation energy of this process should be comparable to the barrier of the $C_2H_6 \rightarrow C_2H_4 + H_2$ reaction, which equals 445.9 kJ mol^{-1} [42]. Indeed, we found that the transition state TS3 corresponding the 1,1-H_2 loss is located 391.4 kJ mol^{-1} above the C_2H_5 radical, that is to say 8.3 kJ mol^{-1} above the entrance channel. As its relative energy towards the ethyl radical is much higher than that of TS1 and TS2: 156.4 and 211.0 kJ mol^{-1}, respectively, this channel will not play any role in this reaction. Previous studies for H_2 loss from C_2H_6 and C_2H_4 have shown that the channels corresponding to a 1,2-H_2 loss are always much higher in energy than those corresponding to a 1,1-H_2 elimination [42,43], therefore these transition states have not been investigated further. This indicates that all channels for a direct H_2 loss are located high in energy. As a consequence the

only observable channel in our experiment is the dissociation of the ethyl radical to form a molecule of ethylene and a hydrogen atom.

3.2. Overall rate constant

The pseudo-first-order decays of CH radical fluorescence signal were monitored at different concentrations of CH_4 or H_2S introduced in large excess. To get rid of the mixing effects, only the last stages of the decay (after 3 cm from the injector exit) have been taken to determine the pseudo-first-order rate constants. The measured rate constants were then corrected from radial and axial diffusions from Keyser's formula [44], as done previously, with good results, for the $CH + NO$ [23] and $CH + O_2$ [45] reactions.

The results of our experiments are displayed in Figs. 3 and 4, where axial and radial corrected pseudo-first-order rate constants are plotted versus the CH_4 and H_2S concentrations, respectively. The main source of errors in our measurements is the important radial and axial diffusions corrections. Moreover, the high wall removal rate constant associated with these diffusions leads to the limited conditions of the plug-flow approximation and the errors quoted take in account these uncertainties. The second-order rate constants are thus $(7.6 \pm 2.0) \times 10^{-11}$, $(2.8 \pm 0.8) \times 10^{-10}$ cm^3 molecule^{-1} s^{-1}, for the $CH + CH_4$ and $CH + H_2S$ reactions,
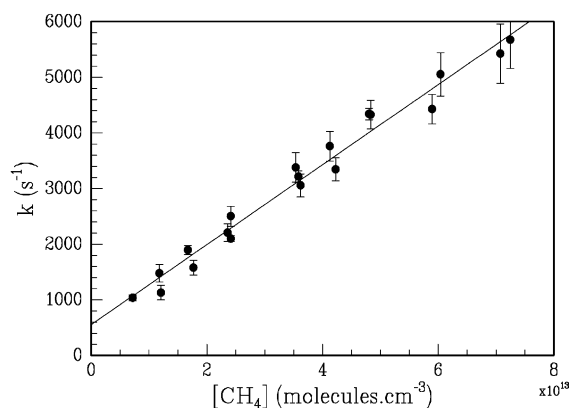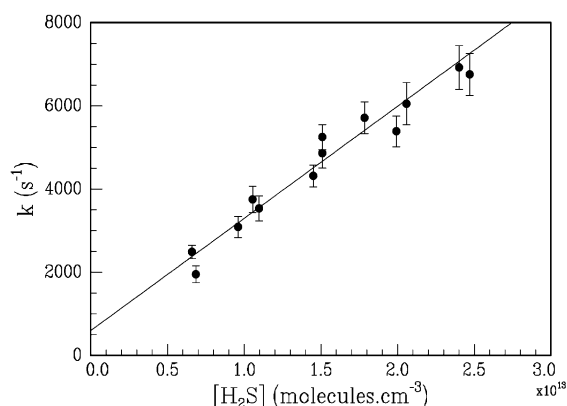

Fig. 4. Plot of the pseudo-first-order rate constant of the $CH + H_2S$ reaction versus the H_2S concentration. The gradient of the fitted line yields to the second-order rate constant, $k = (2.8 \pm 0.8) \times 10^{-10}$ cm^3 molecule^{-1} s^{-1}.

respectively. The present results are in fair agreement with previous measurements [10,13,46,47], even if they are slightly lower.

3.3. Hydrogen atomic production

Relative hydrogen production of the $CH + CH_4$ and $CH + H_2S$ were determined by the ratio to the H production from the $CH + H_2$ reaction by resonance fluorescence in the vacuum ultraviolet. As the H atoms branching ratio is known for the $CH + H_2$ reaction [14], even if this ratio is very dependent on temperature and pressure, the determination of the absolute branching ratios for $CH + CH_4$ and $CH + H_2S$ reactions can thus be worked out.

To measure the relative H atoms production, their fluorescence signals are recorded successively for the three reactions, the CH_4, H_2, and H_2S concentrations being adjusted in order to have equivalent global first-order rate constant. This is possible because our CH production is constant within a period of more than 1 h. This operation was repeated several times, alternately for different CH_4, H_2S, or H_2 concentrations, under different pressures and different $CHBr_3$ concentrations.

As the $CH + H_2$ reaction has a much lower global rate constant than the $CH + CH_4$ and $CH + H_2S$ reactions, we have performed the comparison of $CH + CH_4$ and $CH + H_2$ at 350 K by heating the He buffer gas flow (at 1.4 Torr and 350 K

Fig. 3. Plot of the pseudo-first-order rate constant of the $CH + CH_4$ reaction versus the CH_4 concentration. The gradient of the fitted line yields to the second-order rate constant, $k = (7.6 \pm 2.0) \times 10^{-11}$ cm^3 molecule^{-1} s^{-1}.

$k(CH + H_2) = 2.0 \times 10^{-12}$ [14,15] and $k(CH + CH_4) = 7.5 \times 10^{-11}$ cm^3 molecule^{-1} s^{-1}). An example of the traces of H atoms concentrations, deduced from the fluorescence intensities, versus the distance, i.e., the reaction time, is shown in Fig. 5. In our experimental conditions, we cannot neglect the CH + CH reaction contributions, neither as a direct H atoms source nor as C$_2$H source which could also perturb the H measurement by the C$_2$H + H$_2$, C$_2$H + CH$_4$ or C$_2$H + H$_2$S reactions. The experiments are performed with first-order global rate constant value, for the CH + CH$_4$, CH + H$_2$ and CH + H$_2$S reactions, around 3000 s^{-1} which corresponds to 1 mTorr of CH$_4$, 40 mTorr of H$_2$ or 0.3 mTorr of H$_2$S. Then, considering a thermalized C$_2$H, the first-order global rate constant is around 1200 s^{-1} for the C$_2$H + H$_2$ [48,49] reaction and around 100 s^{-1} for the C$_2$H + CH$_4$ [50] and the C$_2$H + H$_2$S reactions (the C$_2$H + H$_2$S → HS+ C$_2$H$_2$ or H + HCCSH reaction could be estimated close to 10^{-11} cm^3 molecule^{-1} s^{-1}) [51]. The only important secondary source of H atoms is thus the C$_2$H + H$_2$ → H + C$_2$H$_2$ reaction, the two other reactions having too small rate constants compared with the CH reactions (additionally the

C$_2$H + CH$_4$ reaction give only C$_2$H$_2$ and CH$_3$ [52]).

As the H atom and C$_2$H radical production rate by the CH + CH reaction is related to the C$_2$H* chemiluminescence signal (CH + CH → C$_2$H* + H) [24], integration of the C$_2$H* chemiluminescence signal is then proportional to the H and C$_2$H productions. In Fig. 5 is shown the H concentration evolutions from the CH + H$_2$, CH + CH$_4$ and CH + CH reactions. The estimated H contribution from the CH + CH reaction when CH$_4$ or H$_2$ is added is also represented. This contribution is calculated by integrating the C$_2$H* chemiluminescence signal convoluted with a wall loss rate constant of 200 s^{-1}, which is the H atoms wall reaction rate in our reactor. This contribution is then scaled with the H atomic fluorescence signal when only CH radicals are present in the reactor, using the C$_2$H* chemiluminescence integration ratio with and without co-reactants. For the C$_2$H radicals produced by the CH + CH reaction, we consider that all the C$_2$H radicals react with H$_2$ to give C$_2$H$_2$ + H. For thermalized C$_2$H this is done in the first three centimeters. However as C$_2$H is produced in highly vibrationally excited states [24], its reactivity toward H$_2$ is enhanced [53]. In Fig. 6 is shown the corrected H atoms concentrations of the CH + H$_2$ and CH + CH$_4$ reactions, corrections due to the CH + CH → C$_2$H + H and C$_2$H + H$_2$ → C$_2$H$_2$ + H contributions, and also
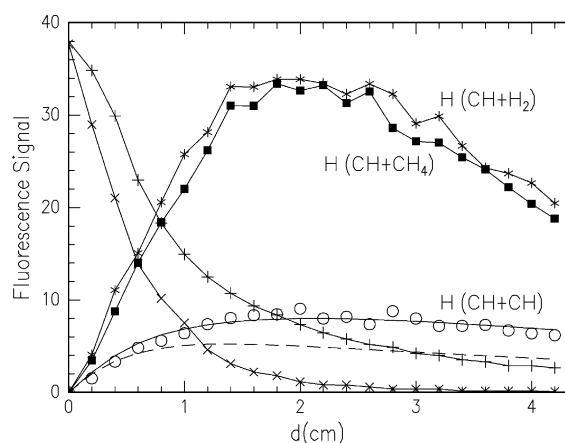

Fig. 5. H atoms fluorescence signal from (◯): CH + CH (when no co-reactant is added); (dashed line): H production from CH + CH, estimated from C$_2$H* chemiluminescence signal, during the CH + CH$_4$ or CH + H$_2$ reaction (see text), (■): CH + CH$_4$, (∗): CH + H$_2$ and C$_2$H* chemiluminescence signal (+): when no co-reactants is added, (×): with CH$_4$ or H$_2$ added, in function of the distance d in the reactor.
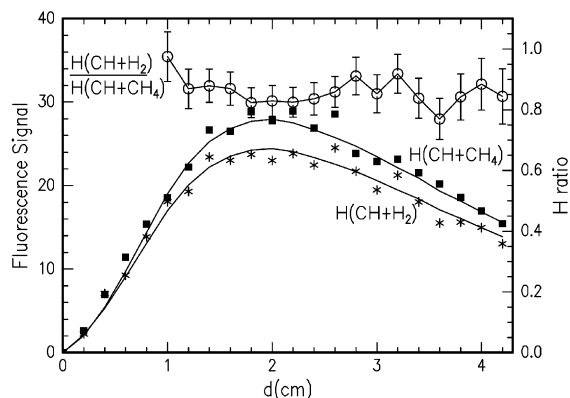

Fig. 6. Corrected H atom concentration from CH + H$_2$ (∗) and CH + CH$_4$ (■) reactions, and the ratio of these two curves (◯), in function of the distance, d, in the reactor.

the ratio of these two curves which is quite constant from the second centimeter to the end of the curve. We must notice that the continuous curve linking the experimental points is the profile of the H atoms production deduced by integrating the experimental decay of CH radicals with additional wall loss of 200 s^{-1} and then by scaling it to the H fluorescence signal, with a converted factor 0.84 less important for $CH + H_2$ reaction than for the $CH + CH_4$ reaction.

To check the validity of this correction, we have measured the evolution of the ratio of [H] production of the $CH + H_2$ and $CH + CH_4$ reactions, in function of the CH initial concentration, at a distance in the reactor of four centimeters. The results, presented in Fig. 7, show a good convergence of the corrected ratio toward 0.84, and underline that the main correction is due to the $C_2H + H_2$ contribution, which could arise 50%. The good convergence of the corrected and raw ratio curves makes us quite confident about the way to estimate the ratio of H production.

Finally we obtain a ratio of H production between the $CH + H_2$ reaction and the $CH + CH_4$ reaction equal to 0.84 ± 0.06. As the H branching ratio of the $CH + H_2$ reaction has been estimated between 81% and 89% at 350 K and 1.4 Torr (81% if we took the Fulle and Hippler data [14] and 89%

if we took the Bronwnsword et al. data [15]), we deduce from the experimental data that the H branching ratio of the $CH + CH_4$ reaction is comprise between 96% and "106"%. To estimate more precisely the H atoms branching ratio, we should use the theoretical information. First, due to the large exothermicity and the low-exit barrier of the $C_2H_4 + H$ channel, the stabilization of C_2H_5 adduct could be neglected, except at very high pressure [13]. Secondly, the endothermic channel $CH_2 + CH_3$ is negligible below 2000 K [13]. And finally, our ab initio calculations show that the $CH + CH_4 \rightarrow C_2H_3 + H_2$ channel, corresponding to the direct reaction $C_2H_5 \rightarrow C_2H_3 + H_2$, is not accessible. Then, we conclude that, at low temperature, the H atom is the exclusive product of the $CH + CH_4$ reaction.

To confirm the use of the $CH + CH_4$ reaction as a calibration of product yield, the $CH + H_2S$ has been studied by comparison with the $CH + CH_4$ reaction. Actually, a recent RRKM study coupled to ab initio calculations [10] estimates a branching ratio for H atoms production close to 100%. As the $CH + H_2S$ reaction is very similar experimental case than $CH + CH_4$ reaction (the $C_2H + H_2S$ reaction contribution is negligible), the correction between the $CH + H_2S$ and the $CH + CH_4$ reaction is only due to the $CH + CH \rightarrow H + C_2H$ reaction. Moreover, as we use equal first-order rate constant, and as the H atoms production are similar for the two reactions, the uncertainties are very small in this case due to equivalent corrections. With a very similar procedure than for the comparison between $CH + CH_4$ and $CH + H_2$ reactions, a ratio of H production between the $CH + H_2S$ reaction and the $CH + CH_4$ reaction is obtained equal to 0.99 ± 0.04. This result is in excellent agreement with the recent RRKM calculations [10] predicting a branching ratio for the $CH_2S + H$ channel equal to 99.6%. It should be noted that this good agreement for this open system (five exit channels) is a good proof of the validity of RRKM calculation when intermediate species have enough long lifetimes (in this case around 2 ps for CH_3S and CH_2SH) for the assumption of a rapid intramolecular transfer leading to energy randomization among internal degrees.
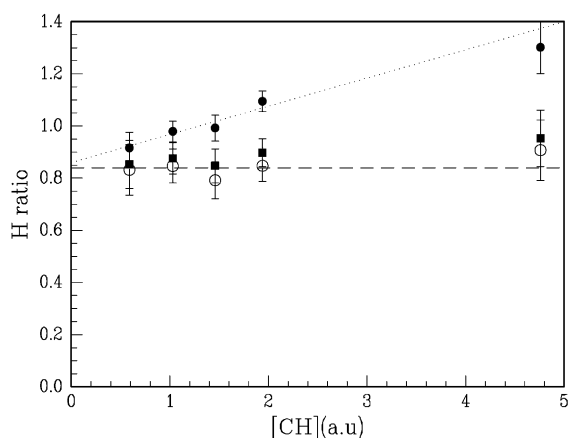

Fig. 7. H atom ratio ($CH + H_2/CH + CH_4$ production) as a function of the initial CH concentration [in arbitrary unit], with no correction (●), corrected for $C_2H + H_2$ (■) reaction and corrected for $C_2H + H_2$ and $CH + CH$ reactions (○).
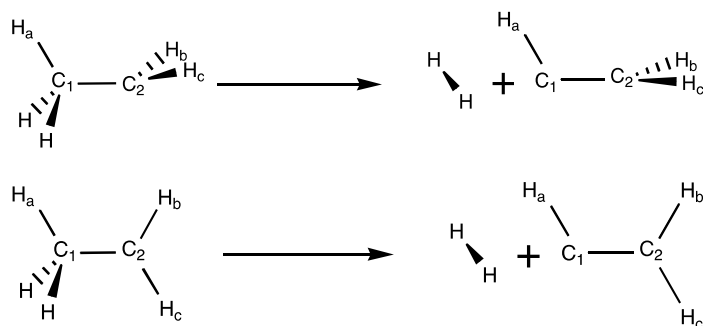
Fig. 8. Paths for the $C_2H_5 \rightarrow C_2H_3 + H_2$ reaction under the C_s symmetry.

4. Conclusions

Despite the fact that we have used the $CH + H_2$ reaction to determine absolute H branching ratios of other reactions, its branching ratio between CH_3 and $CH_2 + H$ channels is very sensitive to several parameters [14], and another reaction is necessary for calibration of H production for CH reactions. From our study, the $CH + CH_4$ reaction is, without any doubt, a much better calibration reaction. First, the possible complications arising from the $CH_2 + CH_3$, C_2H_5 stabilization and $C_2H_3 + H_2$ channels could be ruled out for low-pressure and low-temperature measurements. Secondly, the products of the reaction, C_2H_4 and H, do not react with CH_4 and then secondary reactions are very limited if an excess of CH_4 and a selective source of CH radicals are used. Then we could consider that this reaction proceeds to yield ethene and H atoms exclusively. Moreover, the overall rate constant (and thus detailed rate constants) dependence on temperature is much less critical for the $CH + CH_4$ reaction than for the $CH + H_2$ reaction.

A good illustration is our determination of the H branching ratio of the $CH + H_2S$ reaction, which have been measured equal to $99^{+10}_{-4}\%$, in excellent agreement with recent RRKM calculations [10].

Appendix A

When looking for the transition state leading to $C_2H_3 + H_2$ from the C_2H_5 molecule under the C_s symmetry constraint, two different paths are conceivable as indicated in Fig. 8. In both cases, the $C_1C_2H_a$ fragment lies in the symmetry plane and

the departing H_2 molecule is perpendicular to that plane. In the first channel, the H_bH_c fragment is perpendicular to the symmetry plane whereas it belongs to it in the second channel.

The first channel leads to a non-planar structure corresponding to an excited state of the C_2H_3 molecule. The Woodward–Hoffman correlation diagram corresponding to the second channel is depicted in Fig. 9. This diagram clearly shows that the ground state of C_2H_5 correlates once again with an excited state of the C_2H_3 molecule.
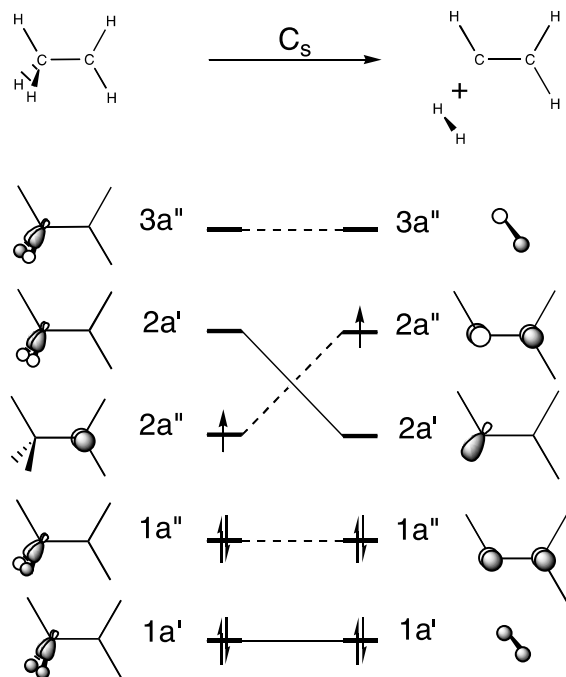

Fig. 9. Woodward–Hoffman correlation diagram for the $C_2H_5 \rightarrow C_2H_3 + H_2$ reaction under the C_s symmetry.

References

[1] W.A. Sanders, M.C. Lin, in: Z.B. Alfassi (Ed.), Chemical Kinetic of Small Organic Radicals, vol. III, CRC, Boca Raton, FL, 1986.

[2] R.P. Wayne, Chemistry of Atmospheres, second ed., Clarendon Press, Oxford, 1991.

[3] J.A. Miller, C.T. Bowman, Prog. Energy Combust. Sci. 15 (1989) 287.

[4] M.W. Chase Jr., NIST-JANAF Thermochemical Tables, fourth ed., J. Phys. Chem. Ref. Data, Monograph 9, 1998, 1.

[5] W. Tsang, in: J.A. Martinho Simoes, A. Greenberg, J.F. Liebman (Eds.), Heats of Formation of Organic Free Radicals by Kinetic Methods in Energetics of Organic Free Radicals, Blackie Academic and Professional, London, 1996, p. 22.

[6] J.S. Pilgrim, C.A. Taatjes, J. Phys. Chem. 101 (1997) 8741.

[7] E.W. Kaiser, T.J. Wallington, J. Phys. Chem. 100 (1996) 4111.

[8] V.D. Knyasev, A. Bencsura, S.I. Stoliarov, I.R. Slagle, J. Phys. Chem. 100 (1996) 11346.

[9] P.W. Seakins, M.J. Pilling, J.T. Niiranen, D. Gutman, L.N. Krasnoperov, J. Phys. Chem. 96 (1992) 9847.

[10] K. Sato, S. Wakabayashi, T. Matsubara, M. Sugiura, S. Tsunashima, Y. Kurosaki, T. Takayanagi, Chem. Phys. 242 (1999) 1.

[11] NIST DataBase (http://www.kinetics.nist.gov).

[12] A. Canosa, I.R. Sims, D. Travers, I.W.M. Smith, B.R. Rowe, Astron. Astrophys. 323 (1997) 644.

[13] M.A. Blitz, D.G. Johnson, M. Pesa, M.J. Pilling, S.H. Robertson, P.W. Seakins, J. Chem. Soc. Faraday Trans. 93 (1997) 1473.

[14] D. Fulle, H. Hippler, J. Chem. Phys. 106 (1997) 8691.

[15] R.A. Brownsword, A. Canosa, B. Rowe, I.R. Sims, W.M. Smith, D.W.A. Stewart, A.C. Symonds, D. Travers, J. Chem. Phys. 106 (1997) 7662.

[16] K. Raghavachari, G.W. Trucks, J.A. Pople, M. Head-Gordon, Chem. Phys. Lett. 157 (1989) 479.

[17] T.H. Dunning Jr., J. Chem. Phys. 90 (1989) 1007.

[18] M.J. Frisch et al., Gaussian 98, Revision A.9, Gaussian Inc., Pittsburgh, PA, 1998.

[19] MOLPRO is a package of ab initio programs written by H.-J. Werner, P.J. Knowles, with contributions from R.D. Amos, A. Bernhardsson, A. Berning, P. Celani, D.L. Cooper, M.J.O. Deegan, A.J. Dobbyn, F. Eckert, C. Hampel, G. Hetzer, T. Korona, R. Lindh, A.W. Lloyd, S.J. McNicholas, F.R. Manby, W. Meyer, M.E. Mura, A. Nicklass, P. Palmieri, R. Pitzer, G. Rauhut, M. Schütz, H. Stoll, A.J. Stone, R. Tarroni, T. Thorsteinsson.

[20] C. Hampel, K. Peterson, H.-J. Werner, Chem. Phys. Lett. 190 (1992) 1.

[21] P.J. Knowles, C. Hampel, H.-J. Werner, J. Chem. Phys. 99 (1993) 5219.

[22] N. Daugey, A. Bergeat, A. Schuck, P. Caubet, G. Dorthe, Chem. Phys. 87 (1997) 222.

[23] A. Bergeat, T. Calvo, N. Daugey, J.-C. Loison, G. Dorthe, J. Phys. Chem. A 102 (1998) 8124.

[24] A. Bergeat, T. Calvo, G. Dorthe, J.-C. Loison, J. Phys. Chem. A 103 (1999) 6360.

[25] M. Born, S. Ingemann, N.M. Nibbering, J. Am. Chem. Soc. 116 (1994) 7210;
E. Tschuikow-Roux, S. Paddison, Int. J. Chem. Kinet. 19 (1987) 15.

[26] Zhou, K.D. Bayes, J. Phys. Chem. 97 (1993) 1896.

[27] A. Bergeat, T. Calvo, G. Dorthe, J.-C. Loison, Chem. Phys. Lett. 308 (1999) 7.

[28] A.M. Mebel, K. Morokuma, M.C. Lin, J. Chem. Phys. 103 (1995) 3440.

[29] J.C. Rienstra-Kiracofe, W.D. Allen, H.F. Schaefer III, J. Phys. Chem. A 104 (2000) 9823.

[30] S. Davis, D. Uy, D.J. Nesbitt, J. Chem. Phys. 112 (2000) 1823.

[31] W.L. Hase, H.B. Schlegel, V. Balbyshev, M. Page, J. Phys. Chem. 100 (1996) 5354.

[32] B.S. Jursic, J. Chem. Soc. Perkin Trans. 2 (1997) 637.

[33] Z.-X. Wang, M.-B. Huang, R.-Z. Liu, Can. J. Chem. 75 (1997) 996.

[34] J. Villà, A. González-Lafont, J.M. Lluch, D.G. Truhlar, J. Am. Chem. Soc. 120 (1998) 5559.

[35] P.J. Marshall, Phys. Chem. A 103 (1999) 4560.

[36] H. Kanamori, Y. Endo, E. Hirota, J. Chem. Phys. 92 (1990) 197.

[37] J.-H. Wang, H.-C. Chang, Y.-T. Chen, Chem. Phys. 206 (1996) 43.

[38] Handbook of Chemistry and Physics, CRC Press, Boca Raton, Florida, 1996.

[39] T.J. Lee, P.R. Taylor, Int. J. Quantum Chem. Quantum Chem. Symp. 23 (1989) 199.

[40] T.J. Lee, J.E. Rice, G.E. Scuseria, H.F. Schaefer, Theor. Chim. Acta 75 (1989) 81.

[41] M.R. Berman, M.C. Lin, Chem. Phys. 82 (1983) 435.

[42] M.S. Gordon, T.N. Truong, J.A. Pople, Chem. Phys. Lett. 130 (1986) 245.

[43] B.S. Jursic, J. Mol. Struc. Theochem 538 (2001) 19.

[44] L.F. Keyser, J. Phys. Chem. 88 (1984) 4750.

[45] A. Bergeat, T. Calvo, F. Caralp, J.-H. Fillon, G. Dorthe, J.-C. Loison, Faraday Disc. 119 (2001) 67.

[46] D.L. Baulch, C.J. Cobos, R.A. Cox, C. Esser, P. Frank, Th. Just, J.A. Kerr, M.J. Pilling, J. Troe, R.W. Walker, J. Warnatz, J. Phys. Chem. Ref. Data 21 (1992) 411.

[47] H. Thiesemann, J. MacNamara, C.A. Taatjes, J. Phys. Chem. A 101 (1997) 1881.

[48] J. Peeters, H. Van Look, B. Ceursters, J. Phys. Chem. 100 (1996) 15124.

[49] B.J. Opansky, S.R. Leone, J. Phys. Chem. 100 (1996) 19904.

[50] B.J. Opansky, S.R. Leone, J. Phys. Chem. 100 (1996) 4888.

[51] By comparison with CH + H_2O reaction.

[52] B. Ceursters, H.M.T. Nguyen, J. Peeters, M.T. Nguyen, Chem. Phys. Lett. 329 (2000) 412.

[53] S. Tasaki, S. Satyapal, R. Bersohn, Can. J. Chem. 72 (1994) 611.